Eur. Phys. J. A (2025) 61:133
https://doi.org/10.1140/epja/s10050-025-01603-8

THE EUROPEAN PHYSICAL JOURNAL A

Regular Article - Experimental Physics

New measurements of (p,xp) and (p,xα) reactions on ^{27}Al at 7.0, 22.0 and 30.0 MeV

D. Gusseinova[1,a], G. Ussabayeva[3,8,9,b], T. K. Zholdybayev[3,9,c], I. Boztosun[1,2,d], Y. Kucuk[1,4,e], A. J. Koning[5,f], Zh. Kerimkulov[3,6], B. Sadykov[3,7,g], A. Temirzhanov[3,7,h], B. Canbula[10,i]

[1] Department of Physics, Akdeniz University, 07058 Antalya, Türkiye
[2] TUBITAK, Temel Bilimler Araştırma Enstitüsü (TBAE), 41470 Kocaeli, Türkiye
[3] Laboratory of Nuclear processes, Institute of Nuclear Physics, Ibragimova 1, 050000 Almaty, Kazakhstan
[4] Turkish Accelerator and Radiation Laboratory (TARLA), 06830 Ankara, Türkiye
[5] International Atomic Energy Agency (IAEA), 1400 Vienna, Austria
[6] L.N. Gumilyov Eurasian National University, 010000 Astana, Kazakhstan
[7] Satbayev University, 050013 Almaty, Kazakhstan
[8] Abai Kazakh National Pedagogical University, Almaty, Kazakhstan
[9] Al Farabi Kazakh National University, Almaty, Kazakhstan
[10] Department of Computer Engineering, Celal Bayar University, Manisa, Türkiye

Received: 1 August 2024 / Accepted: 27 May 2025

Communicated by Alessia Di Pietro

Abstract We present new experimental data for the inclusive (p,xp) and (p,xα) reactions on ^{27}Al target. Double-differential cross sections of (p,xp) at energies 7, 22, 30 MeV and (p,xα) at energies 22, 30 MeV within the angular range of 30°–135° have been measured for the first time. The data has been analyzed by using the exciton model, along with multistep direct and multistep compound models to evaluate the adequacy of the theoretical models in explaining the measured data. Our calculations indicate that the exciton model captures the general trends and oscillatory structures of the spectra at higher proton energies; however, the agreement between theory and experiment remains qualitative, reflecting the inherent complexity of pre-equilibrium reaction mechanisms.

1 Introduction

Experimental information on the double-differential (DDX) and integral cross sections of nucleon-induced reactions in the energy range of 20–200 MeV is becoming increasingly significant in the fields of radioisotope production, radiation safety and protection, development of evaluated nuclear data libraries, and nuclear reaction models [1–3]. The combination of new and previously measured data will improve our understanding of the dynamics of the contribution of pre-equilibrium processes to the total energy spectrum of secondary particles formed with increasing energy.

Pre-equilibrium nuclear reactions occupy an intermediate position between direct nuclear reactions with timescales of $\tau \approx 10^{-22}$ s and reactions involving compound nuclei with timescales of $\tau \approx 10^{-14}$ s [4]. The theoretical description of pre-equilibrium nuclear reactions allows tracing the dynamics of the process as the nuclear system approaches the equilibrium state. These reactions have been described by the Exciton model as well as the modifications of this model [5,6].

The work of Griffin, Cline and Blann [4,7,8] contributed significantly to the development of generalized master equations and stimulated further experimental investigations. These studies yielded two major outcomes: first, they successfully described various features of nuclear reactions-such as cross sections involving nucleons and alpha particles, excitation functions, and angle-integrated particle emis-

All authors contributed equally to this work.

[a] e-mail: gusseinovadi@gmail.com (corresponding author)
[b] e-mail: g.usabayeva@inp.kz
[c] e-mail: zholdybayev@inp.kz
[d] e-mail: boztosun@akdeniz.edu.tr
[e] e-mail: ykucuk@akdeniz.edu.tr
[f] e-mail: a.koning@iaea.org
[g] e-mail: sadykovbm@inp.kz
[h] e-mail: a.temirjanov@inp.kz
[i] e-mail: bora.canbula@cbu.edu.tr

Published online: 12 June 2025

sion spectra-at incident energies around 10 MeV and above. Second, the simplified models proposed in these works provided valuable physical insights into the reaction mechanisms, including the structure of initial configurations, lifetimes of intermediate states, and collision probabilities of excited particles within nuclear matter. Consequently, pre-equilibrium processes have emerged as a key component in achieving a more comprehensive understanding of nuclear reactions [9]. However, the mechanism of pre-equilibrium processes remains insufficiently explored and understood. Further experimental measurements and theoretical developments are still needed in order to enhance our understanding of the reaction mechanism.

So far, several works have been devoted to the study of the reactions (p,xp) and (p,xα) in ^{27}Al. Bertrand and Peelle [10] have measured the energy spectra of secondary particles (p, d, t, ^{3}He, α) at incident proton energies of 29.0 and 62.0 MeV and carried out an analysis within the framework of the intranuclear cascade model. Harada et al. [11] measured the double differential cross-section of the (p,xp) and (p,xα) reactions on ^{27}Al at proton energies of 42 and 68 MeV and compared them to the results of Chadwick et al. [12]. The cross-section measurement results for (p,xp) reactions on ^{27}Al at 90 MeV are presented in [13]. In a recent study, Yamaguchi et al. [3] remeasured the data of Bertrand [10] and Harada et al. [11] at 60° and 150° to investigate discrepancies in the 2–5 MeV energy range. Lewandowski et al. [14] recorded the spectra of α-particles from the reaction with protons on ^{27}Al at $E_p = 72$ MeV. The experimental cross sections were compared with the theoretical calculations within the hybrid model.

Despite several studies on this system, research on ^{27}Al continues, especially at lower energies, to complete the entire picture that would allow conclusions based on fully comprehensive processed data. Therefore, in this work, we have conducted a new experiment to measure the double-differential cross sections (p,xp) and (p,xα) from the interaction of accelerated protons with the ^{27}Al target. We present new data at energies $E_p = 7.0$, 22.0 and 30.0 MeV within the angular range of 30°–135° which has not been extensively investigated to date. In this work, the pre-equilibrium Exciton model and the evaporation theory were used in theoretical calculations.

In the next section, we provide the details of the experimental setup and the experimental results. The theoretical analysis of the experimental results by the pre-equilibrium Exciton Model is given in Sect. 3. Section 4 is devoted to our summary and conclusions.

2 Experiment

The differential cross sections of ^{27}Al(p,xp) and (p,xα) reactions have been measured for the first time at incident proton energies $E_p = 7.0$, 22.0, and 30.0 MeV in the angular range between 30°–135° at the U-150 M isochronous cyclotron of the Institute of Nuclear Physics at Almaty in Kazakhstan.

The scattering chamber, shown in Fig. 1, is located 23.9 m from the exit of the cyclotron beam and has an inner diameter of 60 cm. A particle spectrometer, consisting of a single telescope, was mounted on the rotating cover of the scattering chamber at an angle of 10° to the reaction plane. The spectrometer could be positioned relative to the beam axis at angles θ_{LS} ranging from 10° to 165°, with an accuracy of 0.1°.

The angular uncertainty of the collimator system, positioned just in front of the scattering chamber, determines the dimension of the beam on the target (3 mm). The alignment of the scattering chamber with respect to the beam axis was performed using optical methods. The beam intensity, which ranged from 10 to 50 nA, was adjusted according to the detection angle. A Faraday cup-current integrator system was employed to determine the number of particles impinging on the target. A ^{27}Al foil with a thickness of 3.65 mg/cm^2 and a purity of 98% served as the target. The target thickness was verified by measuring the energy loss of the alpha particles emitted from the ^{226}Ra source.

Reaction products were identified by mass and energy using the (ΔE–E) method, supported by a multidimensional programmable analysis system with ORTEC electronics, as shown in Fig. 2. The signals from the ΔE and E detectors were processed through two spectrometric channels ("E" and "ΔE") and fed into a two-dimensional analyzer equipped with microcontrollers, which works as a remote unit connected to a computer. The system software configured the analyzer's operating modes, and the data were transmitted to the computer for graphical visualization and file storage. The remote unit also included a control pulse counter to estimate errors by comparing the pulse count with the total number of events recorded in the matrix field. In addition, it features an external event counter for signals from the Faraday cup to the digital current integrator (Ortec 439).

To measure the production of charged particles from the (p,xp) reaction at 7 MeV and the (p,xα) reaction at 22 and 30 MeV, silicon detectors with ΔE thicknesses of 25–50 μm and E thicknesses of 2 mm were used. For the reaction (p,xp) at 22 and 30 MeV, a silicon detector with a thickness of 100 μm and a CsI(Tl) scintillator were used. The energy resolution of the measurement system was primarily determined by the beam energy resolution, which was 1% of the initial energy, and the resolution of the detection telescopes. Specifically, the energy resolution was 150 keV for the Si+Si configuration and 300 keV for the Si+CsI configuration. An

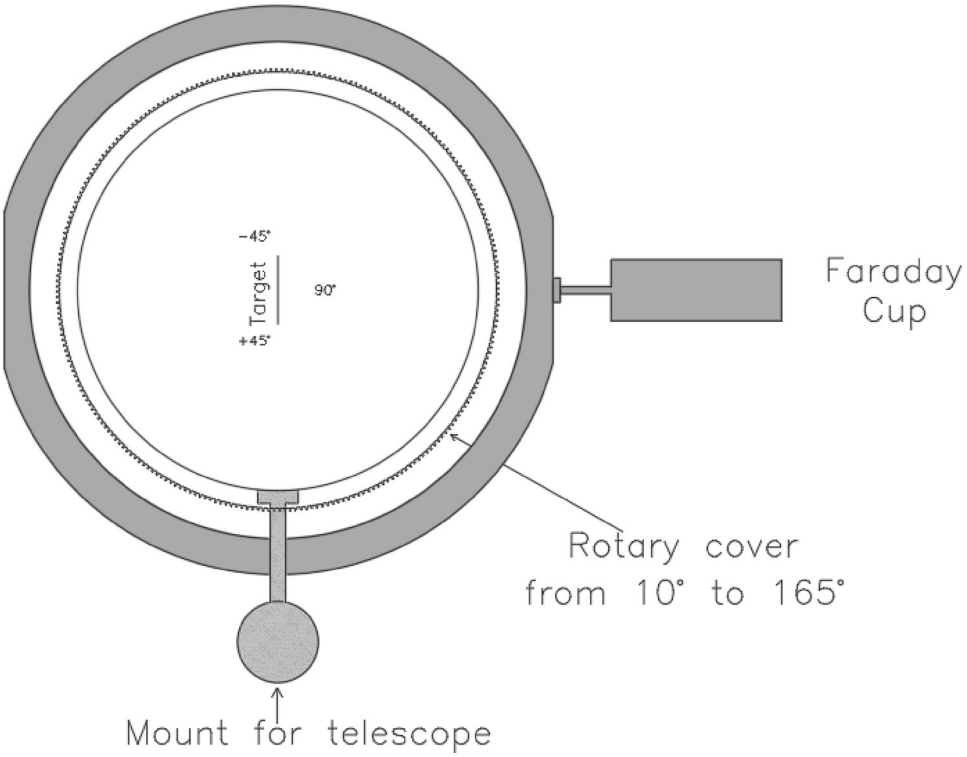

Fig. 1 Scattering chamber used in the experiment. The telescope mount has been installed in a rotary cover, allowing angle measurements from 10° to 165°. Additionally, a rotating target wheel enables switching between different target materials. Faraday Cup is used for absolute current measurement

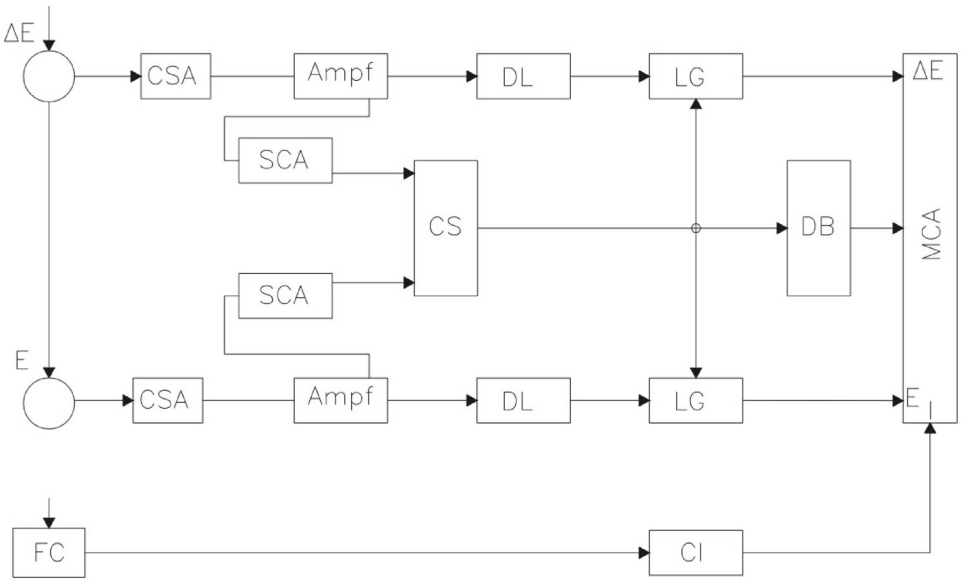

Fig. 2 Particle identification system. *CSA* charge sensitive amplifier, *SCA* single channel analyzer, *Ampf* shaper amplifier, *CS* coincidence scheme, *DL* delay line, *LG* linear gate, *DB* delay block, *MCA* multichannel analyzer, *FC* Faraday cup, *CI* current integrator

example of a two-dimensional plot (ΔE versus E, the yield is on Z) obtained from the telescopes used in the experiments is shown in Figs. 3 and 4. As seen from the figures, the products of the reaction at $E_p = 22$ MeV have been definitively identified.

The systematic errors in the measured cross sections were mainly attributed to uncertainties in the target thickness, which were less than 5%, the calibration of the current integrator, around 1%, and the solid angle of the spectrometer, which had an uncertainty of less than 1.3%. The energy of the accelerated particle beam was measured with an accuracy of 1%. Overall, the total error in the measured cross sections did not exceed 15%.

The double differential cross sections obtained from reactions ^{27}Al(p,xp) and (p,xα) are presented in Figs. 5, 6, 7, 8 and 9. Integrated cross sections over an angle determined from the double-differential cross sections and averaged over the energy range of 0.5 MeV are shown in Figs. 10 and 11. Further details of the experimental procedure are provided in [15–17].

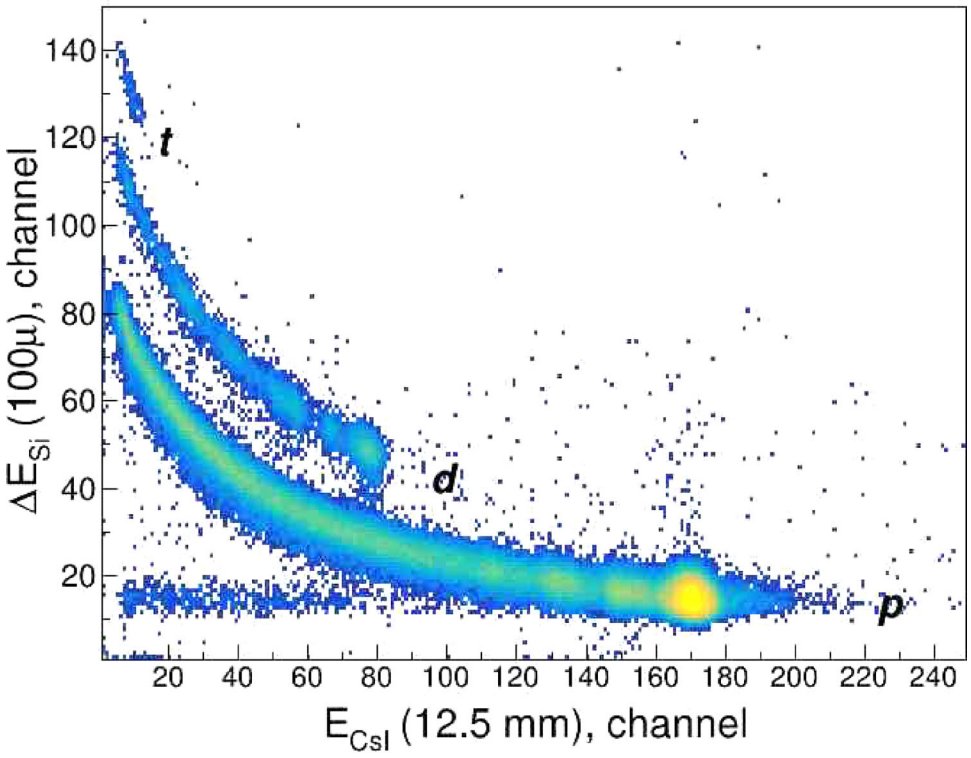

Fig. 3 ΔE–E spectrum of (p,xp) reaction at $E_p = 22$ MeV

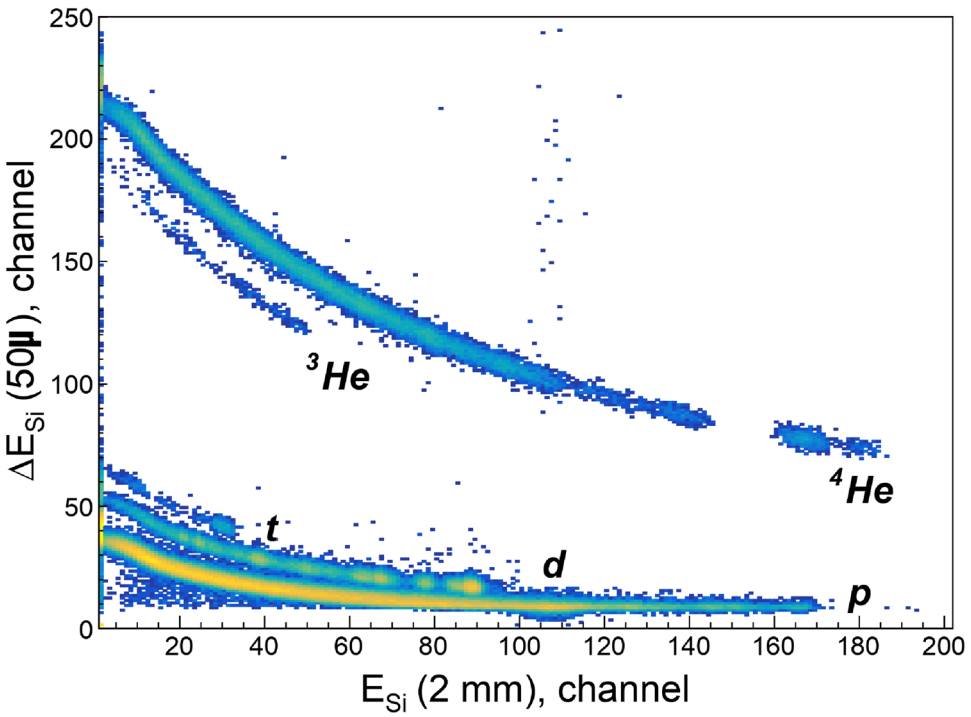

Fig. 4 ΔE–E spectrum of (p,xα) reaction at $E_p = 22$ MeV

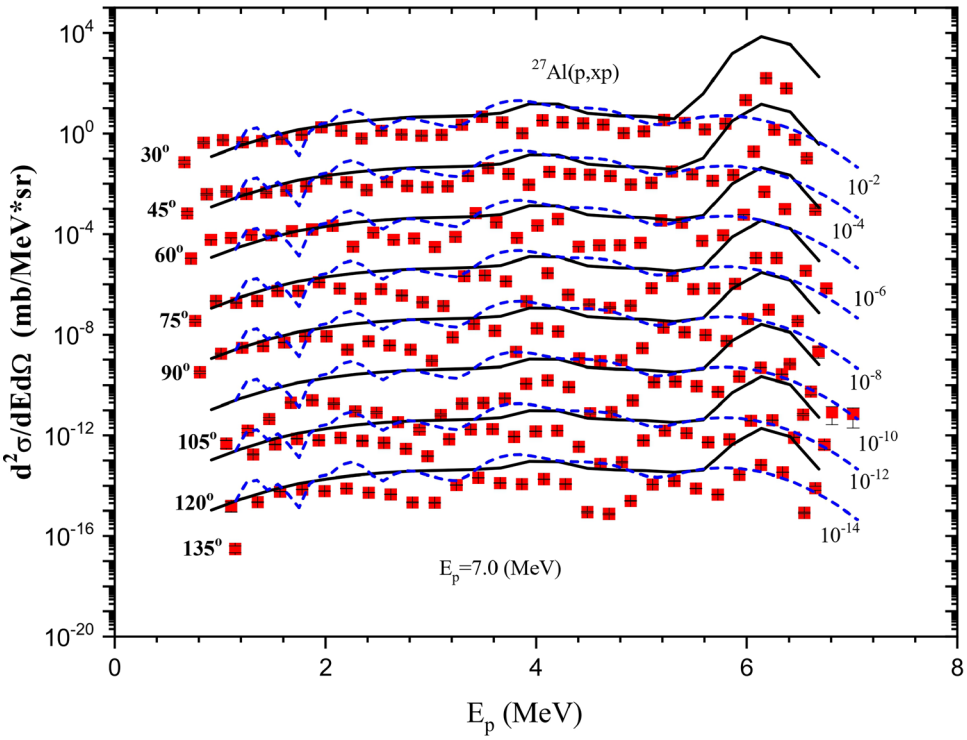

Fig. 5 Double differential cross sections for the ^{27}Al(p,xp) reaction at energy E_p = 7 MeV at 30°, 45°, 60°, 75°, 90°, 105°, 120°, 135°. The solid lines show theoretical results using the first method. Dashed lines show the results using the second model. First model results have been obtained by using the code PRECO while the second model results have been obtained by using the code TALYS

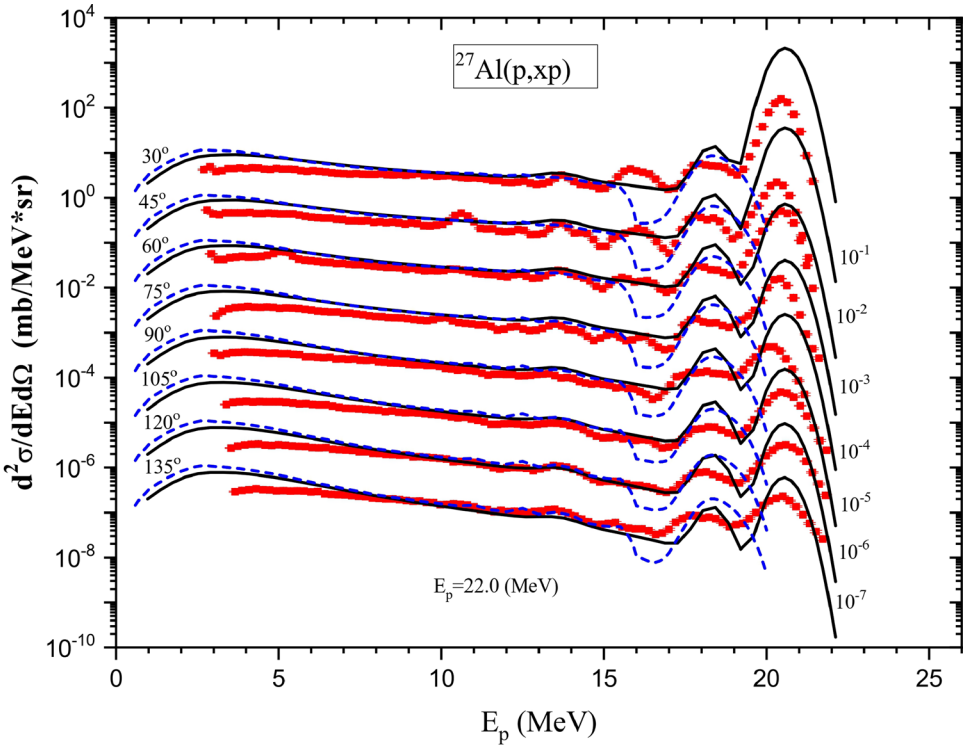

Fig. 6 Double differential cross-sections of the ^{27}Al(p,xp) reaction at energy E_p = 22 MeV at 30°, 45°, 60°, 75°, 90°, 105°, 120°, 135°. The solid lines show theoretical results using the first method. Dashed lines show the results using the second model

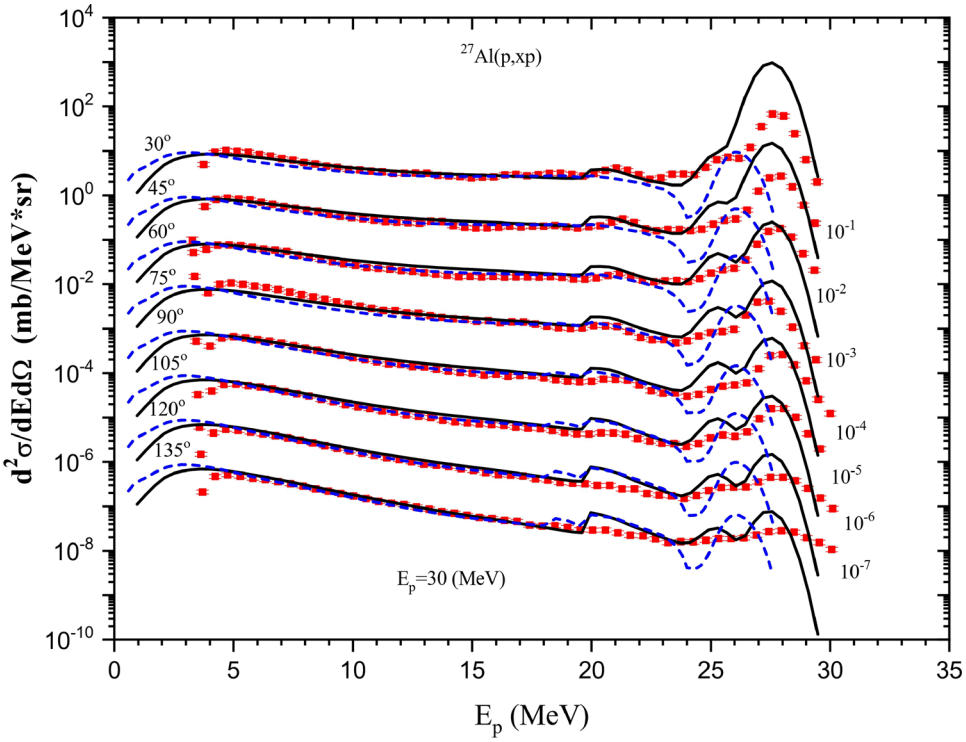

Fig. 7 Double differential cross sections of the ^{27}Al(p,xp) reaction at energy $E_p = 30$ MeV at 30°, 45°, 60°, 75°, 90°, 105°, 120°. The solid lines show theoretical results using the first method. Dashed lines show the results using the second model

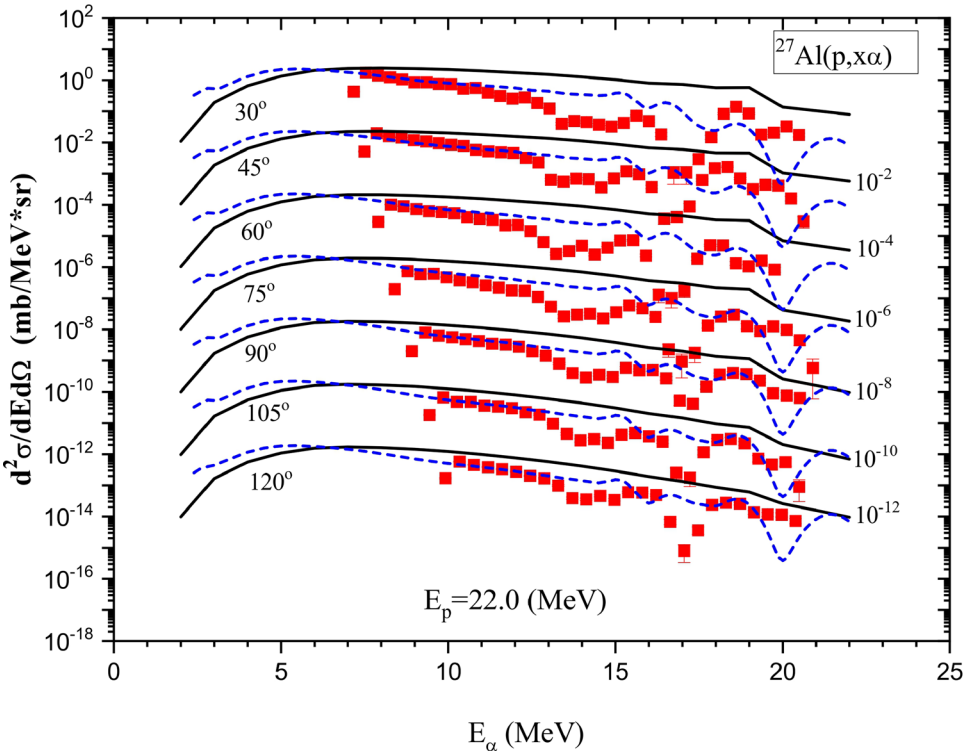

Fig. 8 Double differential cross sections of the ^{27}Al(p,xα) reaction at energy $E_p = 22$ MeV at 30°, 45°, 60°, 75°, 90°, 105°. The solid lines show theoretical results using the first method. Dashed lines show the results using the second model

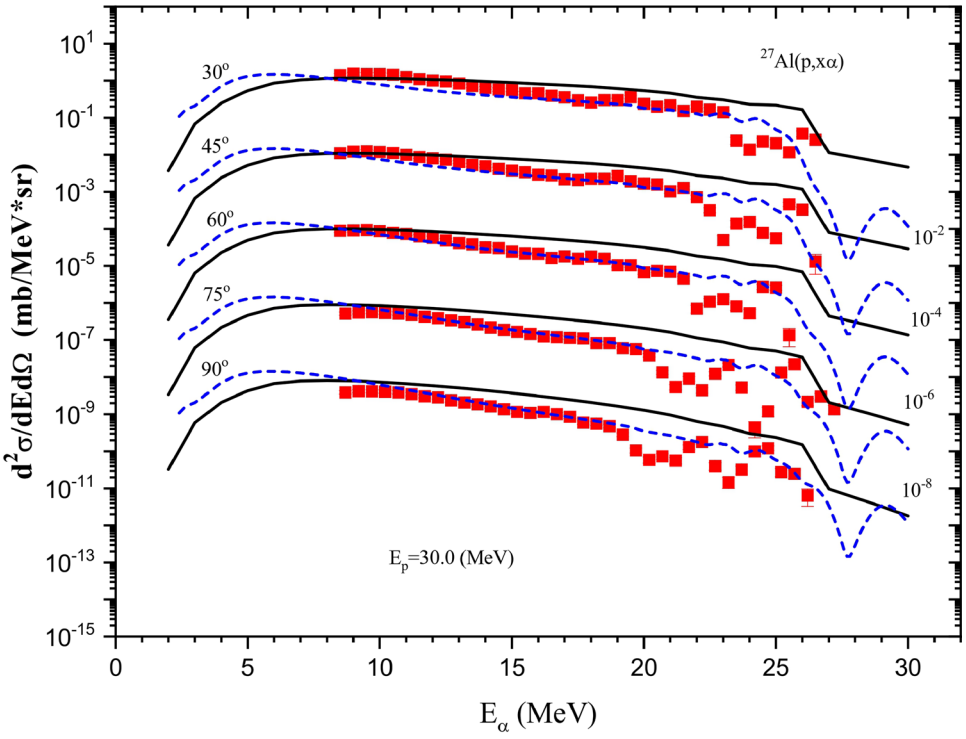

Fig. 9 Double differential cross sections of the ^{27}Al(p,xα) reaction at energy $E_p = 30$ MeV at 30°, 45°, 60°, 75°, 90°.The solid lines show theoretical results using the first method. Dashed lines show the results using the second model

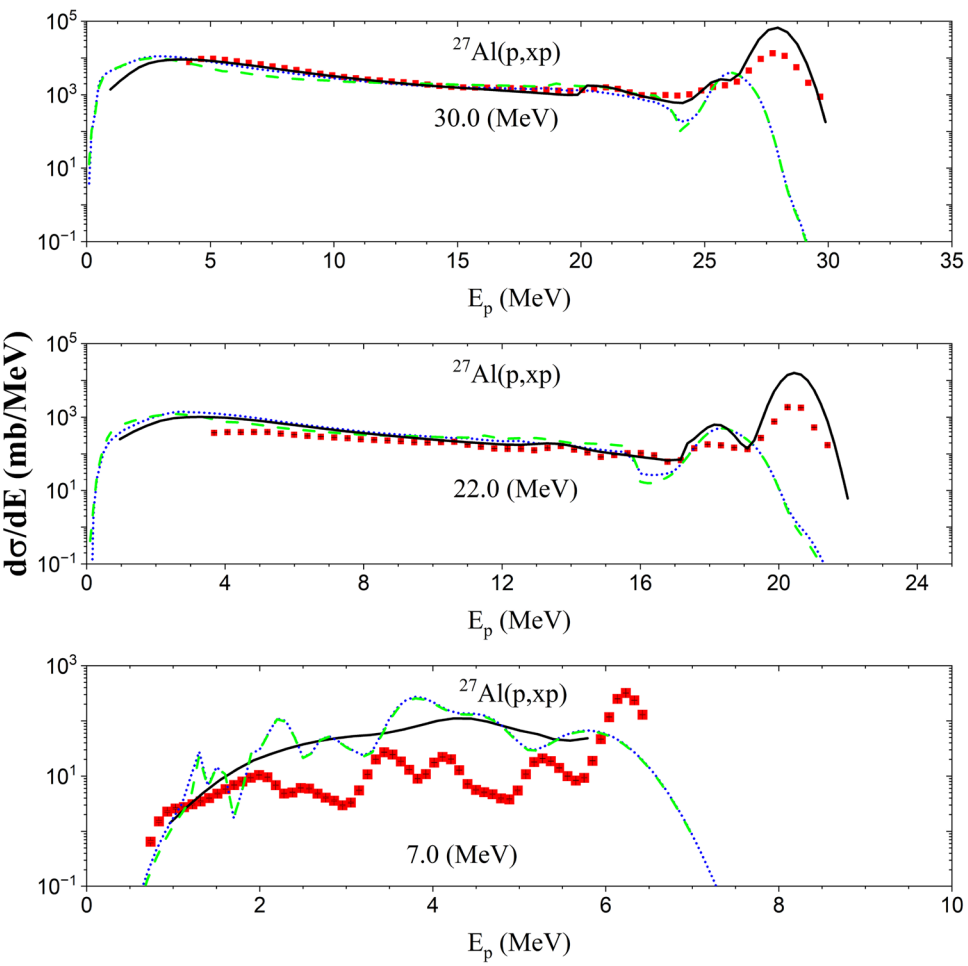

Fig. 10 Angle integrated cross sections of the ^{27}Al(p,xp) at energies $E_p = 7$, 22 and 30 MeV. The solid lines show the results produced by using the exciton model, Weisskopf–Ewing Model, and Bechetti–Greenles parametrization in the optical model (code PRECO), the dotted lines show the results produced by using the exciton model, Hauser–Feshbach model, and Koning–Delaroche parametrization in the optical model (code TALYS). The long dashed lines show the MSD+MSC model calculations using the code TALYS

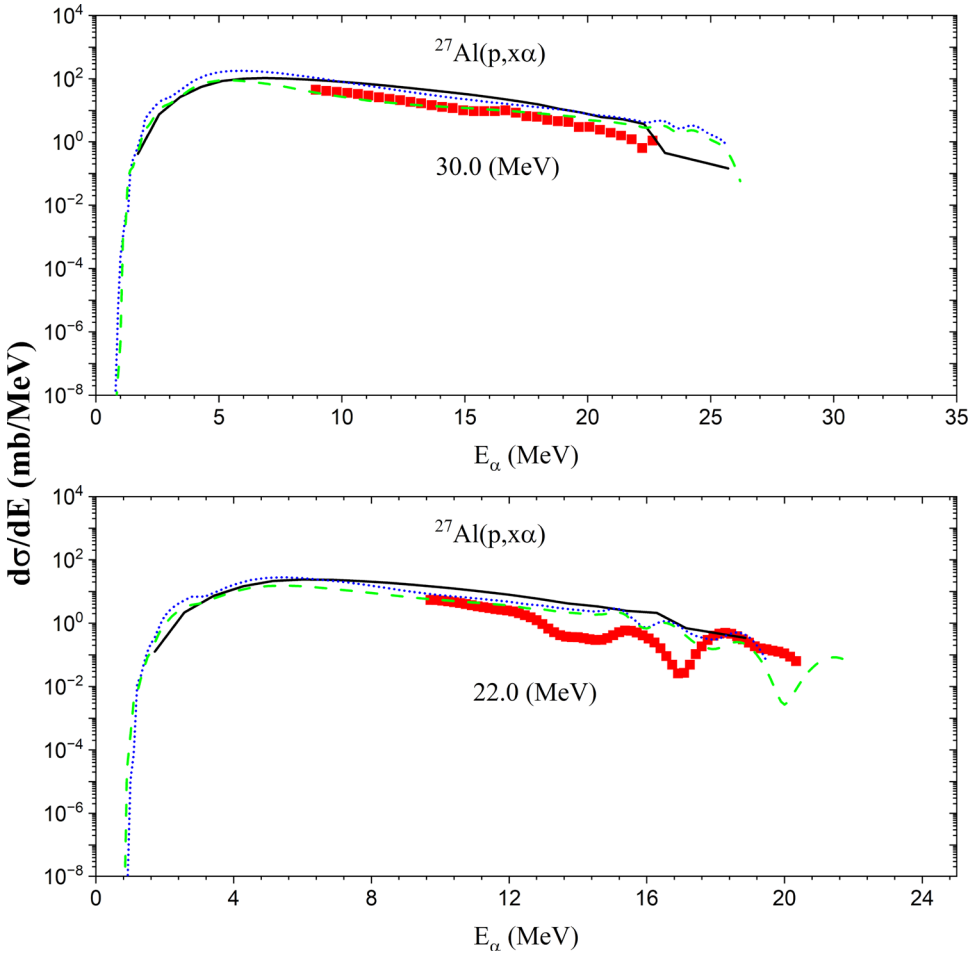

Fig. 11 Angle integrated cross sections of the ^{27}Al(p,xα) Eα = 22 and 30 MeV. The solid lines show the results produced by using the exciton model, Weisskopf–Ewing Model, and Bechetti–Greenles parametrization in the optical model (code PRECO), the dotted lines show the results produced by using the exciton model, Hauser–Feshbach model, and Koning–Delaroche parametrization in the optical model (code TALYS). The long dashed lines show the MSD+MSC model calculations using the code TALYS

3 Theoretical analyses

We calculated double differential and angle-integrated cross sections using two distinct approaches. Both methods account for equilibrium and pre-equilibrium mechanisms in modeling the proton emission spectrum, with the exciton model [18–20] employed to describe the pre-equilibrium process. For the equilibrium contribution, the first method uses the Weisskopf–Ewing evaporation model, while the second relies on the Hauser–Feshbach formalism. These calculations were carried out using the codes PRECO [21] and TALYS 1.95 [22]. An additional distinction between the approaches lies in the optical model potentials: TALYS adopts the global Koning–Delaroche potential [25], whereas PRECO uses the Becchetti–Greenlees parameterization [26].

In the exciton model, the nucleus is characterized by the parameters p_π, h_π, p_ν and h_ν, where p and h denote particle and hole degrees of freedom and π and ν denote proton and neutron degrees of freedom, respectively. They are related to the parameters of the one-component model by the relations p = p_π + p_ν and h = h_π + h_ν. They can also be combined to give the total number n of exciton $n = p + h = p_\pi + h_\pi + p_\nu + h_\nu = n_\pi + n_\nu$. Integration of the main equation over time to the equilibrium time τ_{eq} gives the average lifetime of the exciton state τ, which can be used to calculate the differential cross section [22]. A particle k with energy E_k can be expressed in terms of τ, the cross section for the formation of a compound nucleus σ^{CF}, the particle emission rate W_k and the factor P representing the part of the population that has survived emission from previous states and now passes through the configurations (p_π, h_π, p_ν, h_ν) averaged over time.

$$\frac{d\sigma_k^{PE}}{dE_k} = \sigma^{CF} \sum_{p_\pi = p_\pi^0 \, p_\nu = p_\nu^0}^{p_\pi^{\max}} \sum_{k}^{p_\nu^{\max}} W_k\left(p_\pi, h_\pi, p_\nu, h_\nu, E_k\right) \tau \times \left(p_\pi, h_\pi, p_\nu, h_\nu\right) \times P\left(p_\pi, h_\pi, p_\nu, h_\nu\right) \tag{1}$$

The fragment emission rate W_k, for particles with reduced mass μ_k and spin s_k is [7]:

$$W_k\left(p_\pi, h_\pi, p_\nu, h_\nu, E_k\right) = \frac{2s_k + 1}{\pi^2 h^3} \mu_k E_k \sigma_{k,\,\mathrm{inv}}\left(E_k\right) \times \frac{\omega\left(p_\pi - Z_k, h_\pi, p_\nu - N_k, h_\nu, E^{\mathrm{tot}} - E_k\right)}{\omega\left(p_\pi, h_\pi, p_\nu, h_\nu, E^{\mathrm{tot}}\right)} \tag{2}$$

Table 1 The contributions of direct, compound and pre-equilibrium processes to the total cross-section of ^{27}Al(p,xp) at energies E_p = 7, 22, 30 MeV

E_p, MeV	Total, mb	Direct, mb	Preequilibrium, mb	Compound, mb	Exp. data, mb
7.0	393.8	56.7	4.9×10^{-2}	337.0	147.8± 0.5
22.0	548.8	72.3	2.6×10^{2}	219.5	523.0 ± 1.2
30.0	487.4	60.3	3.2×10^{2}	111.3	712.0 ± 2.0

Table 2 The contributions of direct, compound and pre-equilibrium processes to the total cross-section of ^{27}Al(p,xα) at energies E_p = 22, 30 MeV

E_α, MeV	Total, mb	Direct, mb	Preequilibrium, mb	Compound, mb	Exp. data, mb
22.0	86.5	1.8	21.8	62.9	12.8±0.4
30.0	56.4	0.8	24.6	31.0	19.0± 0.2

where $\sigma_{k,inv}(E_k)$ is the cross section of the inverse process of formation of a compound nucleus, Z_k (N_k) is the proton (neutron) number of the particle emitted, E^{tot} is the total energy of the compound system [24] and $\omega(p_\pi, h_\pi, p_\nu, h_\nu, E^{tot})$ is the particle-hole state density [22]. Proton and neutron single-particle densities are given as g_π = Z/15 and g_ν = N/15 MeV^{-1}, respectively.

We present theoretical calculations obtained using both methods for the double differential cross sections of the (p,xp) reaction at incident energy E_p = 7, 22 and 30 MeV in the Figs. 5, 6 and 7. Theoretical results for (p,xα) at E_p = 22 MeV and 30 MeV are shown in Figs. 8 and 9. As seen from the figures, the first method yields an improved agreement with the (p,xp) data, particularly in reproducing the overall spectral shape, whereas the second method fails to accurately describe the elastic peaks. However, the second method reproduces a better description for the alpha channel. It should be emphasized that the current theoretical approaches provide only qualitative agreement with the experimental data, reflecting the intrinsic complexity of pre-equilibrium reaction mechanisms.

We compare two methods also for the integrated cross sections of the ^{27}Al(p,xp) and ^{27}Al(p,xα) reactions in the Figs. 10 and 11. We have also calculated the contribution of the direct, compound, and pre-equilibrium processes separately by using the second method. The contributions of direct processes such as transfer, knockout, and inelastic scattering have also been determined using direct reaction models. We show the contributions of each process in Table 1 for ^{27}Al(p,xp) and in Table 2 for ^{27}Al(p,xα). As seen from the Table 1, the main contribution to the total cross sections comes from the pre-equilibrium mechanism for the (p,xp) reactions at energies E_p = 22 and 30 MeV, while the contribution of the pre-equilibrium processes is very small at energy E_p = 7 MeV, as expected. For proton bombarding energy below 10 MeV, pre-compound nuclei can be neglected and direct or compound nucleus reactions become dominant. However, for energies above 10 MeV, compound processes are more important as the decay time of the compound nucleus becomes comparable to its internal equilibrium time [23]. Overall, while the use of Exciton and Multistep models provides a useful framework for interpreting the data, the comparison remains qualitative. The observed discrepancies highlight the limitations of current models in fully capturing the complex interplay of reaction mechanisms at these energies. Further development of microscopic models and improved input parameters (e.g., optical potentials, level densities) is essential for achieving a more accurate theoretical description.

4 Results

We have performed a detailed analysis of the ^{27}Al(p,xp) and ^{27}Al(p,xα) reactions at incident proton energies E_p = 7.0, 22.0, and 30.0 MeV. To investigate the underlying reaction mechanisms across these energy ranges, we employed two distinct approaches. In the first approach, the exciton model was used to describe the pre-equilibrium processes, the Weisskopf–Ewing evaporation model for equilibrium processes, and the optical model with Becchetti–Greenlees parametrization for direct processes. The second approach also utilized the exciton model for the pre-equilibrium stage, but incorporated the Hauser–Feshbach model for the compound and the Koning–Delaroche parametrization in the Optical Model for direct processes.

Figure 5 presents the double differential cross sections of the ^{27}Al(p,xp) reaction at incident proton energy E_p = 7 MeV, measured at angles 30°, 45°, 60°, 75°, 90°, 105°, 120°, 135°. The results obtained using the first method (solid lines) and the second method (dashed lines) are compared. As shown in Fig. 5, neither method provides an adequate description of the experimental data at this energy. These results suggest that the models employed are insufficient for accurately reproducing cross sections at low incident energies, indicating the need to account for additional reaction mechanisms or interactions in this energy range. Figures 6 and 7 display the double differential cross sections for protons at energy E_p = 22 and 30 MeV, respectively, at the same angles. At these higher energies, the first

Table 3 The optical potential parameters used in TALYS calculations

Energy (MeV)	V (MeV)	rv (fm)	av (fm)	W (MeV)	rw (fm)	aw (fm)
7.0	27.65	0.813	0.333	0.74	0.813	0.333
22.0	74.28	1.394	0.465	2.33	1.394	0.465
30.0	51.28	1.627	0.599	3.36	1.627	0.599

approach-combining the Exciton model with the Weisskopf–Ewing model and the Becchetti–Greenlees optical potential-demonstrates good agreement with the experimental data. The improved performance is attributed to the dominance of pre-equilibrium processes at higher energies, where the Exciton model effectively captures the high-energy proton emission. In contrast, the second approach-employing the Exciton model with the Hauser–Feshbach model and the Koning–Delaroche optical potential-fails to reproduce the elastic peaks and does not achieve satisfactory agreement at forward angles.

The double differential cross sections of (p,xα) reactions at $E_p = 22$ and 30 MeV, measured at angles 30°, 45°, 60°, 75°, 90°, 105°, are presented in Figs. 8 and 9, respectively. Although the first method accurately reproduces the proton emission spectra, it fails to describe the alpha spectra, particularly at forward angles. This discrepancy may arise from the fundamentally different nature of proton and alpha emission mechanisms. Proton emission is relatively well described by statistical and pre-equilibrium models, while alpha emission is governed by more complex processes, including possible direct mechanisms such as cluster knock-out or transfer, which are not explicitly accounted for in the model. In contrast, the second method (dashed lines) provides an improved description of the alpha spectra, demonstrating better agreement with the experimental data than the first model. It appears that, in the Hauser–Feshbach approach implemented in the TALYS code, the mapping of the pre-equilibrium spectrum onto discrete states-followed by broadening of this strength to simulate experimental conditions-is applied only to outgoing α particles.

We have also calculated the angle-integrated cross sections for ^{27}Al(p,xp) and (p,xα) reactions. The integrated cross section data of protons at $E_p = 7$, 22, and 30 MeV are presented in Fig. 10, with a comparison of results from both methods. Similarly, the integrated cross section for α particles at $E_p = 22$ and 30 MeV has been shown in Fig. 11. It is clearly seen that the first method reproduces only (p,xp) data at $E_p = 22$ and 30 MeV, whereas the second method fails to adequately describe both the (p,xp) and (p,xp) and (p,xα) channels.

Based on these results, we modified the second method by incorporating the multistep direct (MSD) theory of Fesbach, Kerman and Koonin [9,27] and multistep compound (MSC) model instead of the exciton model built in TALYS [28]. As shown in the Figs. 10 and 11, the MSD+MSC model with Hauser–Feshbach and Koning–Delaroche parametrization produces similar results to the exciton model. As seen from the Fig. 11, none of the models used in this study adequately reproduce the (p,xα) data. Since the total reaction cross section remains constant in both cases, a decrease in the pre-equilibrium spectrum for one emitted particle must be offset by an increase for the other, and vice versa. In this case, the MSD-MSC model leads to a better high-energy part of the spectrum for (p,xα). Whether this is a systematic effect, to be expected for many target nuclides, is not yet known.

We also investigated the effect of varying optical potential parameters within the frameworks of the exciton and Hauser–Feshbach models to reproduce the proton spectra. Specifically, we modified the depth, radius, and diffuseness parameters of both the real and imaginary components of the potential. The potential parameters are given in Table 3. This led to some improvement in the calculated spectra at $E_p = 22$ and 30 MeV. However, as shown in Fig. 12, the models still fail to reproduce the elastic peaks. It should be noted that the code TALYS does not account for elastic peaks at these energies, as it considers only non-elastic transitions for incident charged particles. The difference between the results of the first and second models may arise from the fact that TALYS leaves the contribution from the elastic peak out. At $E_p = 22$ and 30 MeV, the real part of the optical potential has a greater influence on the results than the imaginary part. Therefore, we kept the imaginary component fixed, using the Koning–Delaroche parameterization. As shown in the table, the depth and radius of the real potential increase with energy, while the diffuseness parameter decreases at both energies. In contrast, at $E_p = 7$ MeV, both the real and imaginary potential parameters were reduced to account for the oscillatory behavior. Nevertheless, the model still fails to provide a satisfactory fit to the experimental data at this energy.

5 Conclusions

We have presented new experimental data at $E_p = 7.0$, 22.0 and 30.0 MeV within a range of 30°–135° for the inclusive reactions (p,xp) and (p,xα) on nucleus ^{27}Al, which has not been investigated in detail so far. The extension of the pre-equilibrium reactions to this energy region is very important to understand the reaction mechanism of the equilibrium

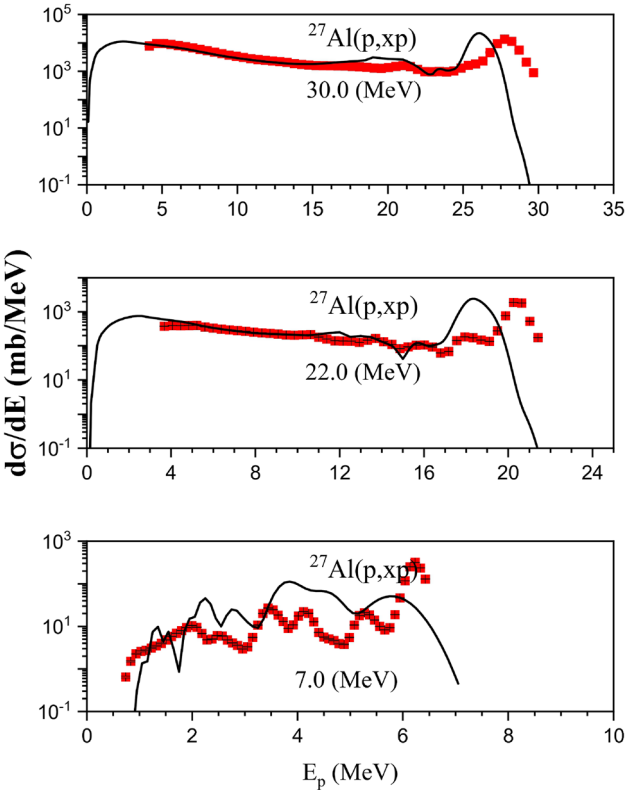

Fig. 12 Angle integrated cross sections of the ^{27} Al(p,xp) produced by using the Optical potential parameters given in Table 3

nuclear reactions as well as to develop theoretical models to explain the measured data. Since there is no experimental data for the protons around 30 MeV, this experimental study is very important for the extension of the pre-equilibrium experiments in this direction to see the mechanism of the reaction and the level of energy dependence. It is also important to assess the adequacy of the aforementioned theoretical models in explaining the measured experimental data. Although our calculations indicate that the exciton model, Weisskopf–Ewing Model, and Becchetti–Greenlees parametrization - corresponding to pre-equilibrium, compound, and direct processes, respectively, provide a reasonable description of the proton and α spectra at $E_p = 22.0$ and 30.0, significant discrepancies persist, and not all theoretical predictions closely align with the experimental data. Also, the proton spectrum at $E_p = 7$ requires more detailed investigation using alternative reaction models.

The theoretical approaches presented in this study are capable of reproducing the gross features of the measured cross-sections. However, the agreement remains largely qualitative, especially in the reproduction of spectral shapes and elastic peaks. At 7 MeV, even qualitative agreement is limited. This reflects the known limitations of current pre-equilibrium models in capturing the full complexity of nuclear reaction mechanisms, highlighting the need for further refinement to achieve a more accurate representation of the experimental data. What requires further investigation is the transition from the compound nuclear reaction mechanism to the pre-equilibrium mechanism as energy increases. While these approaches qualitatively capture this shift, a more detailed analysis is needed to fully understand its impact on the overall reaction dynamics. This transition plays a crucial role in determining the energy dependence of nuclear reactions. It is also clear that the mapping of nuclear transfer reactions, as described by the phenomenological pre-equilibrium model of Kalbach, has room for improvement. In proper pick-up, knock-out, and stripping reactions, the spectroscopic factors for each discrete state must be taken into account. After modeling the direct reaction-using models such as the continuum discretized coupled channels (CDCC) model-the resulting cross sections should be broadened to get a comparison with experimental data. Especially for the (p,xα) reaction, the final results are too structureless. Therefore, a more comprehensive discussion of this shift is necessary to provide a clearer understanding of the underlying physics.

In conclusion, theoretical analysis using the exciton model and related frameworks offers partial insight into the reaction mechanisms, qualitatively reproducing the main features of the spectra. However, quantitative agreement is not achieved, and notable discrepancies-particularly in the shape and magnitude of the cross sections-highlight the current limitations of these models. This emphasizes the necessity for more comprehensive theoretical treatments and improvements in model inputs. It is anticipated that the availability of these experimental data will encourage further theoretical investigations to achieve a more complete understanding of pre-equilibrium nuclear reactions.

Acknowledgements This research was funded by the Science Committee of the Ministry of Science and Higher Education of the Republic of Kazakhstan, grant AP08955998.

Funding Open access funding provided by the Scientific and Technological Research Council of Türkiye (TÜBİTAK).

Data Availability Statement This manuscript has no associated data. [Authors' comment: The experimental nuclear reaction data from this study will be submitted to and made available in the Experimental Nuclear Reaction Data (EXFOR) database maintained by the IAEA Nuclear Data Section (NDS). Once uploaded, the data can be accessed via EXFOR at https://www-nds.iaea.org/exfor.]

Code Availability Statement This manuscript has no associated code/software. [Authors' comment: Code/software sharing is not applicable to this article as no code or software was generated or analysed during the current study.]

Declarations

Conflict of interest There is no declaration of interest.

References

1. K. Kolos, V. Sobes, R. Vogt, C. Romano, M. Smith, L. Bernstein, D. Brown, M. Burkey, Y. Danon, M. Elsawi et al., Current nuclear data needs for applications. Phys. Rev. Res. **4**, 021001 (2022)
2. B. Liu, R. Han, C. Yuan, H. Sun, Z. Chen, G. Tian, F. Shi, X. Zhang, P. Luo, H. Jia, Excitation functions of proton induced reactions on titanium and copper. Appl. Radiat. Isot. **173**, 109713 (2021)
3. Y. Yamaguchi, T. Sanami, Y. Koba, Y. Uozumi, Low-energy-threshold detector for measuring proton spectra at several tens of MeV using Bragg curve spectroscopy. Nucl. Instrum. Methods Phys. Res. Sect. A Accel. Spectrom. Detect. Assoc. Equip. **953**, 163158 (2020)
4. J.J. Griffin, Statistical model of intermediate structure. Phys. Rev. Lett. **17**, 478 (1966)
5. L. Wilets, Surface coupling mechanism for approaching statistical equilibrium in compound nucleus formation, with application to fission. Phys. Rev. **116**, 372 (1959)
6. C. Kalbach, Phenomenology of continuum angular distributions. II. Griffin preequilibrium model. Phys. Rev. C. **23**, 124 (1981)
7. C.K. Cline, M. Blann, The pre-equilibrium statistical model: description of the nuclear equilibration process and parameterization of the model. Nucl. Phys. A **172**, 225–259 (1971)
8. M. Blann, Importance of the nuclear density distribution on pre-equilibrium decay. Phys. Rev. Lett. **28**, 757 (1972)
9. H. Feshbach, A. Kerman, S. Koonin, The statistical theory of multi-step compound and direct reactions. Ann. Phys. **125**, 429–476 (1980)
10. F. Bertrand, R. Peelle, Complete hydrogen and helium particle spectra from 30-to 60-MeV proton bombardment of nuclei with A= 12 to 209 and comparison with the intranuclear cascade model. Phys. Rev. C **8**, 1045 (1973)
11. M. Harada, Y. Watanabe, A. Yamamoto, Y. Tanaka, S. Weili, K. Shin, S. Meigo, O. Iwamoto, H. Nakashima, H. Takada et al., Measurement of double differential cross sections of secondary charged-particles produced by proton-induced reactions at several tens of MeV. J. Nucl. Sci. Technol. **37**, 687–691 (2000)
12. M. Chadwick, P. Young, S. Chiba, S. Frankle, G. Hale, H. Hughes, A. Koning, R. Little, R. MacFarlane, R. Prael et al., Cross-section evaluations to 150 MeV for accelerator-driven systems and implementation in MCNPX. Nucl. Sci. Eng. **131**, 293–328 (1999)
13. J. Wu, C. Chang, H. Holmgren, Charged-particle spectra: 90 MeV protons on Al 27, Ni 58, Zr 90, and Bi 209. Phys. Rev. C **19**, 698 (1979)
14. Z. Lewandowski, E. Loeffler, R. Wagner, H. Mueller, W. Reichart, P. Schober, Analyzing power in the continuum of the (p, xαx) and (p, x) reactions on 12C, 27Al, 58Ni, 90Zr, 209Bi at Ep= 72 MeV. Nucl. Phys. A **389**, 247–260 (1982)
15. A. Duisebaev, B. Duisebaev, T. Zholdybayev, B. Sadykov, K. Ismailov, Inclusive spectra of protons and α particles from reactions induced by protons with an energy of 30.0 MeV on the 209Bi nucleus. Bull. Russ. Acad. Sci. Phys. **78**, 601–604 (2014)
16. A. Duisebayev, K. Ismailov, I. Boztosun, Inclusive spectra of (p, x p) and (p, x d) reactions on 9 0, 9 2 Zr and 92 Mo nuclei at E p= 30.3 MeV. Phys. Rev. C. **67**, 044608 (2003)
17. Y. Kucuk, T. Zholdybayev, B. Canbula, Z. Mukan, B. Sadykov, M. Nassurlla, K. Ismailov, M. Yücel, I. Boztosun, A new proton spectra for nat Cu (p, xp) reaction at E p = 7 and 30 MeV. Eu. Phys. J. A **58**, 97 (2022)
18. P. Hodgson, E. Běták, Cluster emission, transfer and capture in nuclear reactions. Phys. Rep. **374**, 1–89 (2003)
19. C. Kalbach, Preequilibrium reactions with complex particle channels. Phys. Rev. C **71**, 034606 (2005)
20. C. Kalbach, Two-component exciton model: basic formalism away from shell closures. Phys. Rev. C **33**, 818 (1986)
21. C. Kalbach, Users Manual for PRECO-2006, Exciton Model Preequilibrium Nuclear Reaction Code with Direct Reactions. Triangle Universities Nuclear Laboratory, Duke University (2007)
22. A. Koning, D. Rochman, Modern nuclear data evaluation with the TALYS code system. Nucl. Data Sheets **113**, 2841–2934 (2012)
23. H. Nishioka, H. Weidenmiiller, S. Yoshida, Transmission coefficients in the presence of multistep-direct reactions. Z. Phys. A At. Nucl. **336**, 197–202 (1990)
24. J. Dobeš, E. Běták, Two-component exciton model. Z. Für Phys. A At. Nucl. **310**, 329–338 (1983)
25. A. Koning, J. Delaroche, Local and global nucleon optical models from 1 keV to 200 MeV. Nucl. Phys. A **713**, 231–310 (2003). https://www.sciencedirect.com/science/article/pii/S0375947402013210
26. F. Becchetti Jr., G. Greenlees, Nucleon-nucleus optical-model parameters, A> 40, E< 50 MeV. Phys. Rev. **182**, 1190 (1969)
27. R. Lemmer, *Multistep Direct Reactions, Workshop On* (World Scientific, Singapore, 1992)
28. A. Koning, M. Chadwick, Microscopic two-component multistep direct theory for continuum nuclear reactions. Phys. Rev. C **56**, 970 (1997)